ANTIMICROBIAL AGENTS AND CHEMOTHERAPY, Dec. 2008, p. 4308–4314 Vol. 52, No. 12
0066-4804/08/$08.00+0 doi:10.1128/AAC.00656-08

Impact of Self-Assembly Properties on Antibacterial Activity of Short Acyl-Lysine Oligomers[▽]

Hadar Sarig, Shahar Rotem, Lior Ziserman, Dganit Danino, and Amram Mor*

Department of Biotechnology & Food Engineering, Technion-Israel Institute of Technology, Haifa 32000, Israel

Received 18 May 2008/Returned for modification 24 July 2008/Accepted 25 September 2008

We investigated both the structural and functional consequences of modifying the hydrophobic, lipopeptidemimetic oligo-acyl-lysine (OAK) N^{α}-hexadecanoyl-L-lysyl-L-lysyl-aminododecanoyl-L-lysyl-amide ($c_{16}KKc_{12}K$) to its unsaturated analog hexadecenoyl-$KKc_{12}K$ [$c_{16(\omega7)}KKc_{12}K$]. Despite similar tendencies for self-assembly in solution (critical aggregation concentrations, ~10 μM), the analogous OAKs displayed dissimilar antibacterial properties (e.g., bactericidal kinetics taking minutes versus hours). Diverse experimental evidence provided insight into these discrepancies: whereas $c_{16(\omega7)}KKc_{12}K$ created wiry interconnected nanofiber networks, $c_{16}KKc_{12}K$ formed both wider and stiffer fibers which displayed distinct binding properties to phospholipid membranes. Unsaturation also shifted their gel-to-liquid transition temperatures and altered their light-scattering properties, suggesting the disassembly of $c_{16(\omega7)}KKc_{12}K$ in the presence of bacteria. Collectively, the data indicated that the higher efficiency in interfering with bacterial viability emanated from a wobbly packing imposed by a single double bond. This suggests that similar strategies might improve hydrophobic OAKs and related lipopeptide antibiotics.

Synthetic antimicrobial peptidomimetics have recently attracted considerable attention because of their promise to alleviate shortcomings inherent in naturally occurring antimicrobial peptides (AMPs), especially in light of their potential for development as new therapeutic agents (19, 51). Indeed, an extraordinarily large body of experimental work in the past 2 decades has established AMPs as an evolutionarily conserved component of the innate immune response that is capable of targeting a wide range of microorganisms, including enveloped viruses (27), bacteria (13, 48), fungi (8), and mycobacteria (14). In addition to having a role as antimicrobial agents, AMPs may be useful in additional applications, for example, as antitumor agents (3, 21) and immunomodulators (49). Although their detailed mechanism(s) of action is not fully understood, the antimicrobial activities of AMPs are believed to stem from their ability to target and disrupt the integrity of the plasma membrane (20, 41) and/or to interfere with intracellular functions (2, 6). Such a multitarget mode of action is also likely to significantly prevent the emergence of resistance (17, 32). Nevertheless, the potential therapeutic use of AMPs is presently prohibited by several major obstacles pertaining to a less-than-ideal toxicity/bioavailability profile as well as to their relatively high production cost (25).

To overcome these limitations, many have turned their focus to peptidomimetics that reproduce the critical biophysical characteristics of AMPs, such as positive charge, hydrophobicity, and amphipathicity. Peptidomimetics can be based on a variety of oligomers whose primary structures mimic those of peptides through modification of the native peptide backbone, chain extension, and heteroatom incorporation or through de novo-designed polymers. Such structures can ideally circumvent the limitations imposed by the side chains of the 20 main naturally occurring α-amino acid building blocks. Furthermore, the artificial/modified backbone renders most peptidomimetics resistant to degradation enzymes, thereby increasing their stability in vivo (37, 40, 47). For the group with modified native backbones, several strategies were proposed, most of which are based on the preservation of a secondary structure similar to that of natural AMPs. These include the use of stereoisomers of natural peptides (34, 46), the utilization of β-peptides in which the amino group is bonded to the amino acids of β-carbon (26), and the bonding of side chains to backbone amino groups in peptoids (4). In addition, the exploitation of cyclic α-peptides has also been reported (11). Examples of de novo-designed artificial antimicrobial polymers include polyarylamides (45) and polyphenyleneethynylenes (22), in which aromatic monomers are polymerized through amide bonds and utilize a totally abiotic backbone, respectively.

Oligo-acyl-lysines (OAKs) represent a new class of antibacterial (36, 37) and antimalarial (35) peptidomimetic oligomers, composed of alternating aminoacyl chains and cationic amino acids. Like potent AMPs, OAKs can display rapid, nonhemolytic, broad-spectrum microbicidal properties, and they do not induce the emergence of resistance. They therefore appear advantageous over conventional AMPs with respect to in vivo efficacy and safety and may provide a convenient platform for the development of peptide antibiotics. A recent structure activity relationship study performed on a library of >100 OAKs showed that selective antimicrobial activity emerged upon attainment of an optimal hydrophobicity and charge window and that poor antimicrobial performances were linked to the tendency of highly hydrophobic OAKs to aggregate in solution (36). Allegedly, aggregation limits a peptide's interactions with its target(s), thereby reducing antibacterial potency, particularly against gram-negative organisms due to their

* Corresponding author. Mailing address: Laboratory of Antimicrobial Peptides Investigation (LAPI), Department of Biotechnology & Food Engineering, Technion, Haifa 32000, Israel. Phone: (972 4) 8293340. Fax: (972 4) 8293399. E-mail: amor@tx.technion.ac.il.

▽ Published ahead of print on 6 October 2008.

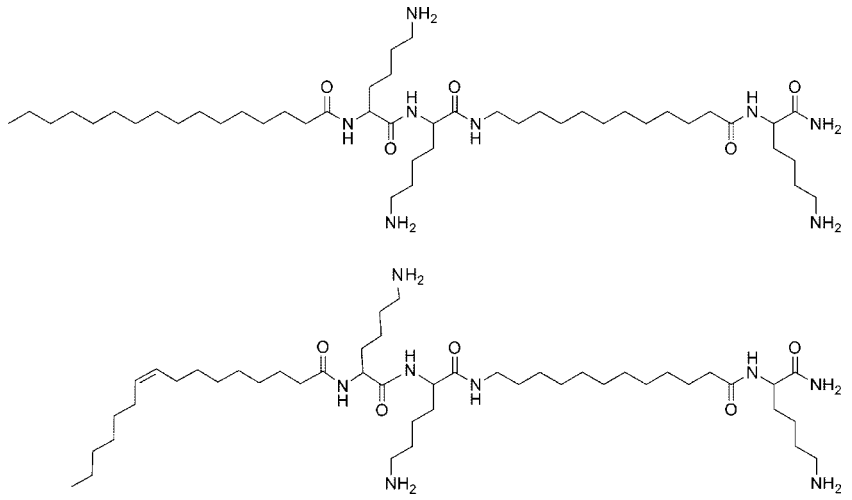

FIG. 1. Molecular structure of the analogous peptide-mimetic OAKs: $c_{16}KKc_{12}K$ (upper structure) and its derivative $c_{16(\omega7)}KKc_{12}K$ (lower structure). β_{12} represents the sequence lysyl-aminododecanoyl-lysyl-amide.

highly impermeable outer membrane (10, 33). This issue is of high relevance due to the wide occurrence of lipopeptide derivatives of host defense peptides in preclinical studies (28) as well as of antibiotics in clinical use (5, 31).

To investigate new means for preventing aggregation, we focused in this study on two new derivatives of the shortest OAK that displayed both antimicrobial activity and a tendency to aggregate in solution ($c_{12}KKc_{12}K$) in previous studies (36). Under the assumption that aggregation is mediated by hydrophobic interactions between the N-terminal acyl moieties, we exacerbated hydrophobicity by substituting the N-terminal dodecanoyl to yield two analogs: hexadecanoyl-K-K-aminododecanoyl-K ($c_{16}KKc_{12}K$) and hexadecenoyl-$KKc_{12}K$ [$c_{16(\omega7)}KKc_{12}K$], shown in Fig. 1. We hypothesized that the unsaturated acyl chain might introduce a structural flaw/perturbation high enough to weaken the characteristically ordered packing of self-assemblies and thereby limit OAKs' aggregation, which might result in improved activity. The reported data demonstrated that while unsaturation did not inhibit aggregation, it nevertheless altered the OAKs' properties in a manner that resulted in improved activity.

MATERIALS AND METHODS

Peptide synthesis. The OAKs were synthesized by the solid-phase method (12) by applying the 9-fluorenylmethyloxy carbonyl (Fmoc) active-ester chemistry (Applied Biosystems model 433A peptide synthesizer) essentially as described previously (35). 4-Methylbenzhydrylamine resin was used to obtain amidated compounds. The fatty acids that were conjugated to each OAK's amino terminus were palmitic acid and palmitoleic (ω7) acid. The crude compounds were purified to chromatographic homogeneity in the range of >95% by reverse-phase high-performance liquid chromatography (HPLC) (Alliance-ZQ Waters). HPLC runs were performed on a C_{18} column (Vydac) with a linear gradient of acetonitrile in water (1%/min); both solvents contained 0.1% trifluoroacetic acid. The purified compounds were subjected to mass analysis in order to confirm their composition and stocked as lyophilized powder at −20°C. Prior to being tested, fresh solutions were prepared in water (mQ; Millipore), briefly vortexed, sonicated, centrifuged, and then diluted in the appropriate medium.

Antibacterial properties. A growth inhibition assay was performed with four bacteria, *Escherichia coli* (ATCC 35218), *Pseudomonas aeruginosa* (ATCC 9027), *Staphylococcus aureus* (ATCC 25923), and *Enterococcus faecalis* (ATCC 29212), grown in LB medium (10 g/liter tryptone, 5 g/liter yeast extract, 5 g/liter NaCl, pH 7.4). MICs were determined by a microdilution assay performed with sterilized 96-well plates and a final volume of 200 μl as follows. Bacteria were grown overnight in LB medium and diluted 10,000-fold in growth medium. One hundred microliters of LB medium containing bacteria (2×10^5 to 4×10^5 CFU/ml) was added to 100 μl of culture medium containing the test compound (0 to 50 μM in serial twofold dilutions). Inhibition of proliferation was determined by optical density measurements (620 nm) after incubation overnight at 37°C. To evaluate bactericidal activity, 20 μl was taken from each well of the MIC experiment and plated on Luria broth agar (LA) for CFU counts after overnight incubation at 37°C. The minimal bactericidal concentration (MBC) is defined as the lowest OAK concentration (μM) causing at least a 99.9% reduction in the number of CFU.

Bactericidal kinetics were assessed as described previously (50). Briefly, bacterial suspensions of *S. aureus* were added to culture medium containing four multiples of the MIC. Bacteria were sampled at various time intervals, subjected to serial 10-fold dilutions, and plated on LA for CFU counts after overnight incubation at 37°C. Statistical data for each experiment were obtained from at least two independent assays performed in duplicate. Hemolytic activity against human red blood cells (RBC) was determined after 3 h of incubation in phosphate-buffered saline (PBS; 50 mM sodium phosphate, 150 mM NaCl, pH 7.4) at 37°C in the presence of a hematocrit of 1%, as described previously (24).

SPR. Binding properties to phospholipid membranes were determined using the BIAcore 2000 optical biosensor system (Biacore Life Science, Uppsala, Sweden) using small unilamellar vesicles composed of 1-palmitoyl-2-oleoyl-sn-glycero-3-phosphocholine (POPC)–1-palmitoyl-2-oleoyl-sn-glycero-3-phosphoglycerol (POPG) (3:1 molar ratio) prepared as described previously (42). Experimental procedures for surface plasmon resonance (SPR), analysis of binding kinetics, and calculation of the resulting affinity constants were performed as described previously (16).

Organization in solution. The OAKs' self-assembly in solution was assessed by light-scattering measurements as described previously (24), using a Jobin-Yvon Horiba Fluorolog-3 system with FluorEssence. Briefly, serial twofold dilutions of the OAKs were prepared in PBS and incubated for 2 h at room temperature, and the light scattering of each dilution was measured by holding both the excitation and the emission at 400 nm (slit width, 1 nm). To describe the dependence of the scattered signal on the OAK concentration, the intensity of scattered light was plotted against the total OAK concentrations. Since the light-scattering signal is proportional to the number of aggregated molecules and the size of the aggregate, the slope is indicative of the aggregation tendency and reveals the aggregation properties, and a slope value above unity indicates the presence of an aggregative form.

DSC experiments. Differential scanning calorimetry (DSC) experiments were carried out using a Microcal VP-DSC-ER calorimeter (Microcal Inc., Northampton, MA) at a scan rate of 30 degrees/h using an OAK concentration of 2 mg/ml in PBS, preheated to 60°C. Data analysis was performed with the Origin 5.0 software (MicroCal).

Microscopy analysis. Unless otherwise stated, all microscopy experiments were performed using the same stock solution (2.4 mM) in PBS, which was

TABLE 1. Biophysical properties of the analogous OAKs

OAK	H^a	Value at a Q of 3 for[b]:								RBC LC_{50}[c]
		E. coli		*P. aeruginosa*		*E. faecalis*		*S. aureus*		
		MIC	MBC	MIC	MBC	MIC	MBC	MIC	MBC	
$c_{16}KKc_{12}K$	62	25–50	>50	25–>50	>50	6–25	25–>50	3–6	25–>50	15 ± 1.5
$c_{16(\omega7)}KKc_{12}K$	57	6	12.5	12.5	50	6	6	3	6	8.5 ± 1

[a] H, hydrophobicity measure as determined by HPLC. The H values represent percentages of the acetonitrile eluent in a C_{18} column.
[b] Q, molecular charge under physiological conditions. MIC, MIC (μM) that induced a 100% inhibition of proliferation after overnight incubation at 37°C.
[c] RBC LC_{50}, OAK concentration (μM) that induced 50% hemolysis of a 1% RBC dilution, after 3 h of incubation in PBS at 37°C. Values were rounded up to the nearest half unit and represent the means ± standard deviations obtained from at least four independent experiments performed in duplicate. The lack of a range indicates consistency.

submitted to a brief vortex, bath sonication, and spin procedure and then incubated (as specified) at room temperature to equilibrate until examination. For light microscopy (LM), a drop (6 to 10 μl) of each sample was applied to a glass slide and observed with a BX51 light microscope (Olympus, Japan) using the phase-contrast mode. Images were digitally recorded with a DP71 camera using the CELL-A software package (Olympus, Japan). Cryogenic transmission electron microscopy (cryo-TEM) specimen preparation was performed by applying a 6-μl drop of the studied solution to a perforated carbon film supported on a 200-mesh TEM copper grid, thinning (blotting), and removing excess solution, and then the sample was vitrified in liquid ethane at its freezing point (−183°C). The procedure was carried out in a controlled-environment vitrification system at 25°C and 100% relative humidity. The vitrified specimens were stored under liquid nitrogen (−196°C) until examination. Negative-stain TEM (NS-TEM) samples were prepared by placing a 6-μl drop of the examined solution on a carbon-coated polymer film supported on a 400-mesh copper grid for 2 min. Then, excess solution was removed with filter paper and the sample was negatively stained with 2% (wt/vol) uranyl acetate. After two more minutes, the grid was blotted again and allowed to dry at room temperature until examination. The samples were examined using a Philips CM120 (Philips, The Netherlands) and a T12-G^2 (FEI, The Netherlands) TEM operated at an accelerating voltage of 120 kV. The vitrified samples were maintained at temperatures below −170°C during sample transfer and observation. In both TEM experiments, images were digitally recorded on cooled charge-coupled-device cameras (Gatan MultiScan 791 or Gatan UltraScan 1000) by using the Gatan Digital Micrograph software package (7). Images were recorded under low-electron-dose conditions to minimize electron beam radiation damage.

RESULTS AND DISCUSSION

Basic biophysical properties. The structures of $c_{16}KKc_{12}K$ and its unsaturated analog $c_{16(\omega7)}KKc_{12}K$ are shown in Fig. 1, while Table 1 summarizes their basic biophysical properties. The data demonstrated that the acyl substitution had profound consequences on the OAKs' activities, which displayed quite distinct antibacterial profiles in terms of potency and specificity, as reflected by their MICs, determined against four representative clinically relevant bacteria: two gram-negative (*E. coli* and *P. aeruginosa*) and two gram-positive (*S. aureus* and *E. faecalis*) bacteria. Thus, $c_{16}KKc_{12}K$ displayed rather poor activity against the gram-negative bacteria, whereas the gram-positive bacteria were more sensitive. Regardless, in all cases, the potency of this OAK was difficult to define since the MIC kept fluctuating (even after six independent experiments). Such a fluctuation—which is expected from aggregative compounds—would not be worth mentioning had it been observed with $c_{16(\omega7)}KKc_{12}K$ as well. In contrast, the unsaturated analog displayed reduced hydrophobicity (as determined by HPLC [Table 1]) that correlated with stable MICs on all tested bacteria. Moreover, $c_{16(\omega7)}KKc_{12}K$ revealed an overall enhanced antibacterial potency.

Table 1 also compares the MBCs of the analogous OAKs. While the higher MBCs indicated that the OAKs exerted an essentially bacteriostatic effect at the MIC, the MBC experiments also confirmed that $c_{16(\omega7)}KKc_{12}K$ is endowed with enhanced bactericidal activity, especially against the gram-positive bacteria (as validated in Fig. 2B). In fact, $c_{16(\omega7)}KKc_{12}K$ also displayed a higher hemolytic activity than $c_{16}KKc_{12}K$ as assessed against human RBC in terms of the concentration that induced 50% hemoglobin leakage (50% lethal concentration). Incidentally, although such OAKs may be difficult to use in systemic therapeutic applications due to their anticipated toxicity, these simple and inexpensive compounds could be useful in topical treatments of resilient infections and eventually in other antibacterial applications, such as in cosmetics, food, or pharmaceutical technologies (43, 44).

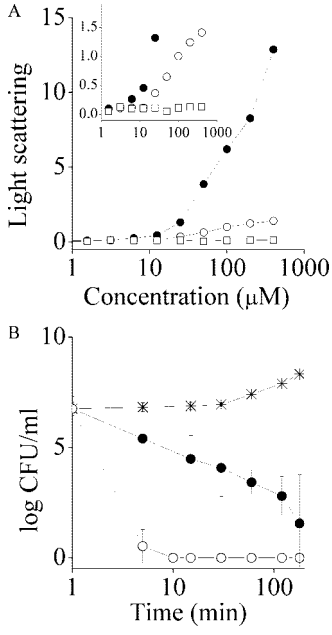

FIG. 2. Light scattering and bactericidal activities of the analogous OAKs. (A) Dose dependence of the light-scattering intensities of PBS solutions of $c_{16}KKc_{12}K$ (filled circles), $c_{16(\omega7)}KKc_{12}K$ (open circles), and $KKc_{12}K$ as the negative control (open squares). (Inset) Tenfold magnification of the y axis. (B) Bactericidal kinetics of 12.5 μM $c_{16}KKc_{12}K$ assayed against *S. aureus* (filled circles), $c_{16(\omega7)}KKc_{12}K$ (open circles), and the untreated control (stars). Bacteria were sampled at the designated time periods, subjected to serial 10-fold dilutions, and plated on LA dishes for a CFU count after overnight incubation at 37°C.

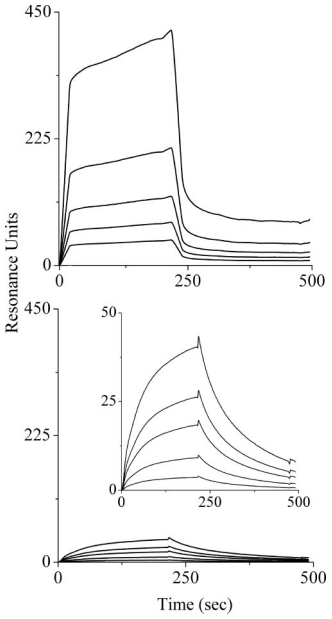

FIG. 3. Representative binding sensorgrams at high and low concentrations of OAKs. Shown are binding curves (association/dissociation rates) of high and low concentrations (upper and lower panels, respectively) of $c_{16}KKc_{12}K$ in PBS, pH 7.4, to a bilayer composed of POPC-POPG (ratio of 3:1) using the L1 chip. Low concentrations were 0.16, 0.31, 0.62, 1.25, and 2.5 μM. High concentrations were 3.1, 6.25, 12.5, 25, and 50 μM. The curves with greater intensity correspond to higher peptide concentrations. Each sensorgram represents an average curve for two independent injections of each concentration. The calculated binding constants from these experiments are summarized in Table 2. (Inset) View of the binding curves with smaller values on the *y* axis.

The combined results were thus contradictory as to the effect of acyl substitution: antibacterial results suggested that the unsaturated acyl inhibited aggregation. But if this were true, one would expect to see reduced hemolytic activity, since reduced hydrophobicity generally correlates with reduced hemolysis (1, 39) whereas increased hemolysis generally correlates with aggregation (23, 38). We contemplated therefore a third possibility: unsaturation might not inhibit aggregation but alter it in some way. This view was supported by a variety of experimental results, including light-scattering properties, bactericidal kinetics, and binding parameters, as described below.

Light-scattering properties. Figure 2A shows the dose-dependent light-scattering of PBS solutions of three analogs, $c_{16}KKc_{12}K$, $c_{16(\omega7)}KKc_{12}K$, and, as a control, $KKc_{12}K$ (a truncated analog lacking the N-terminal acyl), for which the critical aggregation concentration (CAC) was estimated upon divergence from linearity. Accordingly, both acylated analogs were found to aggregate at approximately 10 μM, but at each concentration thereafter, $c_{16}KKc_{12}K$ displayed significantly higher light-scattering intensities, reflecting a difference in its aggregate properties.

Bactericidal kinetics. The OAKs' bactericidal properties were compared at a concentration equal to four multiples of the MIC and assessed against *S. aureus*, for which the MICs were the most similar (Table 1). As shown in Fig. 2B, $c_{16(\omega7)}KKc_{12}K$ displayed radically faster bactericidal kinetics, reducing the CFU count by 6 log units within 10 min (compared to 360 min) of incubation. These results, while appearing to support the option of reduced/altered aggregation, may suggest that the observed potencies were linked to either different efficiencies (e.g., different affinities of binding to bacterial targets) or an altogether different mechanism of action. We therefore attempted to compare the OAKs' binding properties to those of a negatively charged phospholipid bilayer that mimics bacterial plasma membranes (POPC/POPG ratio, 3:1) (42) using the SPR technology.

Binding properties. Because of the alleged tendency for aggregation, the binding experiments were conducted with two series of concentrations (low and high) for each OAK. Typical association and dissociation kinetic curves for $c_{16}KKc_{12}K$ at high and low concentrations are shown in Fig. 3 (upper and lower panels, respectively), and the derived binding constants are summarized in Table 2. When analyzed by the two-step binding model (16), the affinity constants were rather similar at low concentrations but drastically different at high concentrations. Thus, the adhesion and insertion affinities of $c_{16}KKc_{12}K$ were reduced by 5- and 100-fold, respectively, resulting in an overall apparent affinity constant ($K_{apparent}$) that was lower by 3 orders of magnitude than that at the low concentrations.

One way to interpret these results is picturing that, at low concentrations, the $c_{16}KKc_{12}K$ monomers are attracted by electrostatic forces to the anionic model membrane (high $K_{adhesion}$). Upon adhesion, the lipophilic monomers expressed a 10-fold-higher preference for the inserted state (high $K_{insertion}$), i.e., they preferred to be embedded within the bilayer, than for the superficially attached state. When the OAK is present in an aggregated form, however (i.e., above the CAC), the OAK aggregate was attracted by weaker electrostatic forces that allowed superficial adherence (low $K_{adhesion}$), but the aggregate was unable to embed itself (low $K_{insertion}$). These discrepancies were not observed with $c_{16(\omega7)}KKc_{12}K$, whose affinity constants at both concentrations (low and high series) remained unchanged and very much comparable to the low concentrations of the saturated OAK. Therefore, under the assumption that the OAKs indeed target the bacterial plasma membrane (37), these results combine with the observed rapid bactericidal kinetics (which is also consistent with a membrane-disruptive mechanism) to support the possibility of similar mechanisms of action, since at least at concentrations below the CAC, the OAKs displayed comparable binding properties, which suggested that the observed differences

TABLE 2. OAKs' binding properties to a model phospholipid membrane[a]

OAK	Concn range[b]	$K_{adhesion}$ (M^{-1})	$K_{insertion}$	$K_{apparent}$ (M^{-1})
$c_{16}KKc_{12}K$	Low	2.2×10^6	10.3	8.3×10^7
	High	4.3×10^5	0.1	4.3×10^4
$c_{16(\omega7)}KKc_{12}K$	Low	2.1×10^6	8.1	1.7×10^7
	High	1.5×10^6	10.1	4.5×10^7

[a] SPR affinity constants were calculated from an average of five duplicated binding curves for each OAK.

[b] Low concentrations were 0.16, 0.31, 0.62, 1.25, and 2.5 μM. High concentrations were 3.1, 6.25, 12.5, 25, and 50 μM. χ^2 (reflecting the best fit) ranged between 2.5 and 10.

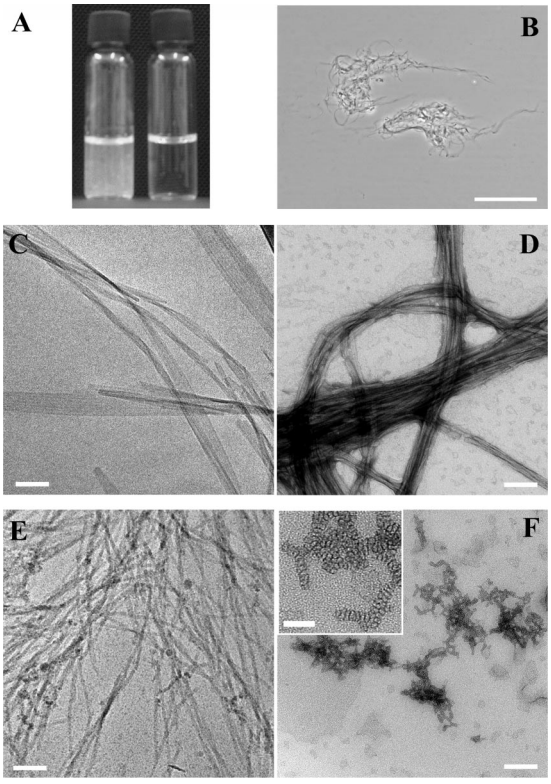

FIG. 4. Evidence for differences in self-assembly properties. (A) Solutions of $c_{16}KKc_{12}K$ (left) and $c_{16(\omega7)}KKc_{12}K$ (right) in PBS (2.4 mM) after 1 h of incubation at room temperature. (B) LM image of a $c_{16}KKc_{12}K$-PBS solution (50 μM). Bar = 50 μm. (C) cryo-TEM image of a $c_{16}KKc_{12}K$-PBS solution (2.4 mM). Bar = 100 nm. (D) NS-TEM image of a $c_{16}KKc_{12}K$-PBS solution (50 μM). Bar = 100 nm. (E) cryo-TEM image of a $c_{16(\omega7)}KKc_{12}K$-PBS solution (2.4 mM). Bar = 100 nm. (F) NS-TEM image of a $c_{16(\omega7)}KKc_{12}K$-PBS solution (50 μM). Bar = 100 nm. (Inset) Fourfold increase of the image in panel F. Bar = 25 nm.

stemmed from differences in their supramolecular organizations in solution rather than from distinct mechanisms of action. These considerations prompted us to conduct additional investigations which might evidence differences in the OAKs' aggregation properties that explain the differential antibacterial properties.

Organization studies. A difference between the OAKs' aggregative features was obvious by eye observation of freshly prepared stock solutions (2 mg/ml = 2.4 mM) in PBS at room temperature. While at first, both OAKs seemed well soluble, $c_{16}KKc_{12}K$ solutions became turbid within 1 hour, unlike the $c_{16(\omega7)}KKc_{12}K$ solution (Fig. 4A). We next visualized the aggregates' morphology by light and electron microscopy techniques. Observation of freshly prepared PBS solutions at concentrations of 2.4 mM (not shown) and 50 μM by LM revealed the $c_{16}KKc_{12}K$ solutions to be populated with amorphous clumps that reached hundreds of microns in length (Fig. 4B). These OAK chunks seem to represent a thicket of microfibers that are crumpled together. In contrast, no signs of aggregation were detected in LM observations of $c_{16(\omega7)}KKc_{12}K$, even after 10 days of incubation (not shown).

cryo-TEM investigation, however, confirmed that, on the nano-scale, both OAKs were indeed aggregated. At 2.4 mM, both samples contained nano-fibers, but they were of distinct morphologies: $c_{16(\omega7)}KKc_{12}K$ created a thin network of interconnected fibers (Fig. 4E), while $c_{16}KKc_{12}K$ formed wider and stiffer fibers that entangled rather than interconnected (Fig. 4C). Since low μM solutions were too diluted for cryo-TEM observation, we used the NS-TEM technique, which allows the study of lower concentrations. The results obtained with $c_{16}KKc_{12}K$ further supported the cryo-TEM findings and linked the nano- and microscale results, in general. Figure 4D shows how $c_{16}KKc_{12}K$ fibers entangle to create small-scale thickets, similar to those shown in the LM image. NS-TEM also confirmed that the thicket is made of bundles of fibers, as observed in cryo-TEM (Fig. 4D). The fibers have a parallel organization that form "ropes" that can reach a thickness on the micron scale (not shown). Such variable ropes meet at a "nucleation point" and form the basis for the microscale aggregates shown in the LM image. Except for the numbers and sizes of the thickets, NS-TEM results with 50 μM and 2.4 mM solutions were practically identical. NS-TEM results with $c_{16(\omega7)}KKc_{12}K$ in 50 μM (Fig. 4F) as well as in 2.4 mM (not shown) solutions showed only interconnected fine nanofibers, also in line with the cryo-TEM results (Fig. 4E). However, as shown in the magnified insert, a morphological change occurred in the fibers, which appeared as tight contiguous helical fibers (telephone cord like). Although we cannot rule out the possibility of an artifact resulting from the OAK interacting with the stain, these results nevertheless support a genuine qualitative difference in the OAKs' aggregative organizations, where the self-assembly of the unsaturated analog appears to be relatively less rigid (more loosely packed?) than the fibers formed by $c_{16}KKc_{12}K$.

To test this hypothesis, we compared the changes in light-scattering intensity following the addition of bacteria (*S. aureus* at 10^5 CFU/ml) to each OAK solution. Figure 5A demonstrates that adding bacteria to the $c_{16(\omega7)}KKc_{12}K$ (but not the $c_{16}KKc_{12}K$) solution reduced the light-scattering intensity nearly by half (56%) after 10 min, suggesting that the presence of bacteria induced disassembly of the unsaturated OAK only. This possibly implies that, unlike self-assemblies of $c_{16}KKc_{12}K$, those of $c_{16(\omega7)}KKc_{12}K$ can readily be disassembled, namely, because of altered supramolecular packing imposed by the unsaturated acyl. To further verify this possibility, we compared the analogous OAK behaviors by determining DSC measurements at a concentration of 2.4 mM in PBS. As shown in Fig. 5B, a transition temperature (51°C ± 0.4°C) was observed for $c_{16}KKc_{12}K$ but not for $c_{16(\omega7)}KKc_{12}K$, thus providing additional support to the view that the self-assembly of $c_{16(\omega7)}KKc_{12}K$ is maintained by significantly weaker forces.

Hence, while both OAKs can self-assemble into nano-structures, only the $c_{16}KKc_{12}K$ fibers can form higher-order assemblies (ropes). The ropes serve as building units for microscale growth that evolve into big thickets or "chunks," as can be observed in the LM and NS-TEM images. These findings are not surprising, because it is well established that unsaturated hydrocarbon chains in general and fatty acids in particular have much looser molecular packing than do saturated hydrocarbon chains, mostly because of the kink in the hydrocarbon chain at the *cis* double-bond sites (9, 29). This explains their low melting and boiling temperatures compared with those of their

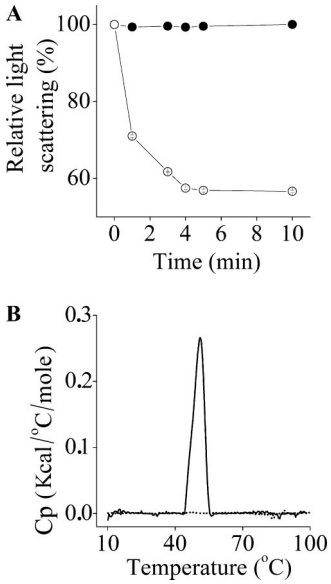

FIG. 5. Evidence for tighter versus looser packing of the self-assemblies. (A) Shown are the changes in light-scattering intensities after *S. aureus* (10^5 CFU/ml) was added to the OAK solutions (200 μM) in PBS. (B) DSC measurements upon heating of 2.4 mM solutions of the analogous OAKs. Shown are the results of representative runs from at least two independent experiments showing a gel-to-liquid transition temperature of 51°C ± 0.4°C for $C_{16}K$-β_{12} (solid line) but not for $c_{16(\omega7)}KKc_{12}K$ (dotted line). Cp, heat capacity; kcal, kilocalories.

analogous saturated fatty acids. For example, the melting points of palmitic acid and palmitoleic acid (9-*cis*-hexadecenoic acid) are 63 and 0.5°C (29), respectively. Further validation of the inherent differences between saturated and unsaturated OAK aggregates was provided by the DSC results. The peak around 50°C, which the literature refers to as the gel-to-liquid transition temperature (9, 29), indicates that the hydrocarbons of $c_{16}KKc_{12}K$ are in the gel phase at room temperature. This means that the molecules are tightly packed and create stiff structures that can hold a long-range order (9, 15). This allows $c_{16}KKc_{12}K$ aggregates to grow from the nano-scale range into the microscale range. On the other hand, no such transition peak was found for $c_{16(\omega7)}KKc_{12}K$. Due to the low melting point of palmitoleic acid, it is reasonable to assume that its gel-to-liquid transition temperature is below 10°C, which was the lower limit of the DSC apparatus that we used. This means that the hydrocarbons in the $c_{16(\omega7)}KKc_{12}K$ aggregates are fluid at room temperature. The molecular degree of freedom is much greater in the fluid phase. Consequently, $c_{16(\omega7)}KKc_{12}K$ fibers do not grow into the microscale range (15).

Taken together, the data suggested that, in aqueous solution, $c_{16}KKc_{12}K$ forms "tighter" and more-stable aggregates even in the presence of bacteria for which they indeed present a high binding affinity as monomers, and this probably enables them to superficially adhere to bacterial cell wall surfaces as an aggregate. However, in order to affect bacterial viability, the OAKs must reach at least the plasma membrane (assuming the presence of a membrane-disruptive mechanism). In contrast, although $c_{16(\omega7)}KKc_{12}K$ also tends to aggregate in solution, its self-assembly is not as tight and its molecules are somewhat available for interaction with target cells. This interaction appears to lead to disassembly, as previously described for natural AMPs (18), and consequently provides a basis for the observed efficient interference with bacterial viability. According to this view, aggregation per se might even potentiate an OAK's action by facilitating a local concentration of a large number of OAK molecules on the target cells (bacteria or RBC) (18, 33). This view also explains the fact that both analogs displayed overall weaker activities against the gram-negative bacteria than against the gram-positive bacteria (more so for $c_{16}KKc_{12}K$). The highly hydrophilic and anionic external membrane of gram-negative bacteria is more likely to imprison cationic aggregates, thus preventing their progression toward internal targets.

In conclusion, it is well established that along with positive charge and amphipathic organization, hydrophobicity is a critical force driving the antimicrobial activities of host defense peptides. However, it is now equally clear that excess hydrophobicity can also be responsible for reduced potency due to aggregation in aqueous media. There is therefore a major interest in finding efficient means that would prevent the deleterious consequences of aggregation while preserving antimicrobial properties (i.e., without significantly reducing hydrophobicity). In this study, we propose to overcome the consequences of aggregation in hydrophobic OAKs by replacing an acyl moiety with an unsaturated fatty acid. This subtle change in the OAK sequence is shown to be responsible for improved antibacterial properties. Thus, aggregation need not necessarily to be utterly eliminated. This investigation also raised the possibility that the unsaturated acyl altered the aggregates' properties by causing them to form looser assemblies, which can disassemble upon contact with bacteria. These findings suggest therefore that the use of unsaturated fatty acids might represent an effective means of increasing the repertoire of available antimicrobial agents by improving potency and/or the specificities of many aggregated OAKs (36), lipopeptides (30), and antibiotics (5, 31).

ACKNOWLEDGMENTS

This research was supported by the Israel Science Foundation (grant 283/08) and BiolineRx (grant 2006992).

REFERENCES

1. **Avrahami, D., Z. Oren, and Y. Shai.** 2001. Effect of multiple aliphatic amino acids substitutions on the structure, function, and mode of action of diastereomeric membrane active peptides. Biochemistry **40:**12591–12603.
2. **Boman, H. G., B. Agerberth, and A. Boman.** 1993. Mechanisms of action on *Escherichia coli* of cecropin P1 and PR-39, two antibacterial peptides from pig intestine. Infect. Immun. **61:**2978–2984.
3. **Chen, J., X. M. Xu, C. B. Underhill, S. Yang, L. Wang, Y. Chen, S. Hong, K. Creswell, and L. Zhang.** 2005. Tachyplesin activates the classic complement pathway to kill tumor cells. Cancer Res. **65:**4614–4622.
4. **Chongsiriwatana, N. P., J. A. Patch, A. M. Czyzewski, M. T. Dohm, A. Ivankin, D. Gidalevitz, R. N. Zuckermann, and A. E. Barron.** 2008. Peptoids that mimic the structure, function, and mechanism of helical antimicrobial peptides. Proc. Natl. Acad. Sci. USA **105:**2794–2799.
5. **Cotroneo, N., R. Harris, N. Perlmutter, T. Beveridge, and J. A. Silverman.** 2008. Daptomycin exerts bactericidal activity without lysis of *Staphylococcus aureus*. Antimicrob. Agents Chemother. **52:**2223–2225.
6. **Cudic, M., and L. Otvos, Jr.** 2002. Intracellular targets of antibacterial peptides. Curr. Drug Targets **3:**101–106.
7. **Danino, D., A. Bernheim-Groswasser, and Y. Talmon.** 2001. Digital cryogenic transmission electron microscopy: an advanced tool for direct imaging of complex fluids. Colloids Surf. A *183***-185:**113–122.
8. **De Lucca, A. J., and T. J. Walsh.** 1999. Antifungal peptides: novel therapeutic compounds against emerging pathogens. Antimicrob. Agents Chemother. **43:**1–11.

9. **Evans, F. E., and H. Wennerstrom.** 1999. The colloidal domain. VCH, New York, NY.
10. **Feder, R., A. Dagan, and A. Mor.** 2000. Structure-activity relationship study of antimicrobial dermaseptin S4 showing the consequences of peptide oligomerization on selective cytotoxicity. J. Biol. Chem. **275:**4230–4238.
11. **Fernandez-Lopez, S., H. S. Kim, E. C. Choi, M. Delgado, J. R. Granja, A. Khasanov, K. Kraehenbuehl, G. Long, D. A. Weinberger, K. M. Wilcoxen, and M. R. Ghadiri.** 2001. Antibacterial agents based on the cyclic D,L-alpha-peptide architecture. Nature **412:**452–455.
12. **Fields, G. B., and R. L. Noble.** 1990. Solid phase peptide synthesis utilizing 9-fluorenylmethoxycarbonyl amino acids. Int. J. Pept. Protein Res. **35:**161–214.
13. **Friedrich, C. L., D. Moyles, T. J. Beveridge, and R. E. Hancock.** 2000. Antibacterial action of structurally diverse cationic peptides on gram-positive bacteria. Antimicrob. Agents Chemother. **44:**2086–2092.
14. **Fu, L. M.** 2003. The potential of human neutrophil peptides in tuberculosis therapy. Int. J. Tuberc. Lung Dis. **7:**1027–1032.
15. **Fuhrhop, J. H., and W. Helfrich.** 1993. Fluid and solid fibers made of lipid molecular bilayers. Chem. Rev. **93:**1565–1582.
16. **Gaidukov, L., A. Fish, and A. Mor.** 2003. Analysis of membrane-binding properties of dermaseptin analogues: relationships between binding and cytotoxicity. Biochemistry **42:**12866–12874.
17. **Ge, Y., D. L. MacDonald, K. J. Holroyd, C. Thornsberry, H. Wexler, and M. Zasloff.** 1999. In vitro antibacterial properties of pexiganan, an analog of magainin. Antimicrob. Agents Chemother. **43:**782–788.
18. **Ghosh, J. K., D. Shaool, P. Guillaud, L. Ciceron, D. Mazier, I. Kustanovich, Y. Shai, and A. Mor.** 1997. Selective cytotoxicity of dermaseptin S3 toward intraerythrocytic Plasmodium falciparum and the underlying molecular basis. J. Biol. Chem. **272:**31609–31616.
19. **Hancock, R. E., and H. G. Sahl.** 2006. Antimicrobial and host-defense peptides as new anti-infective therapeutic strategies. Nat. Biotechnol. **24:**1551–1557.
20. **Heller, W. T., A. J. Waring, R. I. Lehrer, and H. W. Huang.** 1998. Multiple states of beta-sheet peptide protegrin in lipid bilayers. Biochemistry **37:**17331–17338.
21. **Hoskin, D. W., and A. Ramamoorthy.** 2008. Studies on anticancer activities of antimicrobial peptides. Biochim. Biophys. Acta **1778:**357–375.
22. **Ishitsuka, Y., L. Arnt, J. Majewski, S. Frey, M. Ratajczek, K. Kjaer, G. N. Tew, and K. Y. Lee.** 2006. Amphiphilic poly(phenyleneethynylene)s can mimic antimicrobial peptide membrane disordering effect by membrane insertion. J. Am. Chem. Soc. **128:**13123–13129.
23. **Javadpour, M. M., and M. D. Barkley.** 1997. Self-assembly of designed antimicrobial peptides in solution and micelles. Biochemistry **36:**9540–9549.
24. **Kustanovich, I., D. E. Shalev, M. Mikhlin, L. Gaidukov, and A. Mor.** 2002. Structural requirements for potent versus selective cytotoxicity for antimicrobial dermaseptin S4 derivatives. J. Biol. Chem. **277:**16941–16951.
25. **Latham, P. W.** 1999. Therapeutic peptides revisited. Nat. Biotechnol. **17:**755–757.
26. **Liu, D., and W. F. DeGrado.** 2001. De novo design, synthesis, and characterization of antimicrobial beta-peptides. J. Am. Chem. Soc. **123:**7553–7559.
27. **Lorin, C., H. Saidi, A. Belaid, A. Zairi, F. Baleux, H. Hocini, L. Belec, K. Hani, and F. Tangy.** 2005. The antimicrobial peptide dermaseptin S4 inhibits HIV-1 infectivity in vitro. Virology **334:**264–275.
28. **Makovitzki, A., D. Avrahami, and Y. Shai.** 2006. Ultrashort antibacterial and antifungal lipopeptides. Proc. Natl. Acad. Sci. USA **103:**15997–16002.
29. **Markley, K. S.** 1960. Fatty acids: their chemistry, properties, production, and uses. Interscience, New York, NY.
30. **Marynka, K., S. Rotem, I. Portnaya, U. Cogan, and A. Mor.** 2007. In vitro discriminative antipseudomonal properties resulting from acyl substitution of N-terminal sequence of dermaseptin s4 derivatives. Chem. Biol. **14:**75–85.
31. **Montero, A., J. Ariza, X. Corbella, A. Domenech, C. Cabellos, J. Ayats, F. Tubau, C. Ardanuy, and F. Gudiol.** 2002. Efficacy of colistin versus beta-lactams, aminoglycosides, and rifampin as monotherapy in a mouse model of pneumonia caused by multiresistant *Acinetobacter baumannii*. Antimicrob. Agents Chemother. **46:**1946–1952.
32. **Navon-Venezia, S., R. Feder, L. Gaidukov, Y. Carmeli, and A. Mor.** 2002. Antibacterial properties of dermaseptin S4 derivatives with in vivo activity. Antimicrob. Agents Chemother. **46:**689–694.
33. **Oren, Z., J. C. Lerman, G. H. Gudmundsson, B. Agerberth, and Y. Shai.** 1999. Structure and organization of the human antimicrobial peptide LL-37 in phospholipid membranes: relevance to the molecular basis for its non-cell-selective activity. Biochem. J. **341:**501–513.
34. **Oren, Z., and Y. Shai.** 1997. Selective lysis of bacteria but not mammalian cells by diastereomers of melittin: structure-function study. Biochemistry **36:**1826–1835.
35. **Radzishevsky, I., M. Krugliak, H. Ginsburg, and A. Mor.** 2007. Antiplasmodial activity of lauryl-lysine oligomers. Antimicrob. Agents Chemother. **51:**1753–1759.
36. **Radzishevsky, I. S., T. Kovachi, Y. Porat, L. Ziserman, F. Zaknoon, D. Danino, and A. Mor.** 2008. Structure-activity relationships of antibacterial acyl-lysine oligomers. Chem. Biol. **15:**354–362.
37. **Radzishevsky, I. S., S. Rotem, D. Bourdetsky, S. Navon-Venezia, Y. Carmeli, and A. Mor.** 2007. Improved antimicrobial peptides based on acyl-lysine oligomers. Nat. Biotechnol. **25:**657–659.
38. **Radzishevsky, I. S., S. Rotem, F. Zaknoon, L. Gaidukov, A. Dagan, and A. Mor.** 2005. Effects of acyl versus aminoacyl conjugation on the properties of antimicrobial peptides. Antimicrob. Agents Chemother. **49:**2412–2420.
39. **Rotem, S., I. Radzishevsky, and A. Mor.** 2006. Physicochemical properties that enhance discriminative antibacterial activity of short dermaseptin derivatives. Antimicrob. Agents Chemother. **50:**2666–2672.
40. **Rotem, S., I. S. Radzishevsky, D. Bourdetsky, S. Navon-Venezia, Y. Carmeli, and A. Mor.** 2008. Analogous oligo-acyl-lysines with distinct antibacterial mechanisms. FASEB J. **22:**2652–2661.
41. **Shai, Y.** 2002. Mode of action of membrane active antimicrobial peptides. Biopolymers **66:**236–248.
42. **Shalev, D. E., S. Rotem, A. Fish, and A. Mor.** 2006. Consequences of N-acylation on structure and membrane binding properties of dermaseptin derivative K_4-S4-(1-13). J. Biol. Chem. **281:**9432–9438.
43. **Singh, P., and S. S. Cameotra.** 2004. Potential applications of microbial surfactants in biomedical sciences. Trends Biotechnol. **22:**142–146.
44. **Solans, C., N. Azemar, M. R. Infante, and T. Warnheim.** 1989. Phase behavior of cationic lipoamino acid surfactant systems, p. 70–75. *In* H. G. Kilian and G. Lagaly (ed.), Progress in colloid and polymer science. Springer, Berlin, Germany.
45. **Tew, G. N., D. Liu, B. Chen, R. J. Doerksen, J. Kaplan, P. J. Carroll, M. L. Klein, and W. F. DeGrado.** 2002. De novo design of biomimetic antimicrobial polymers. Proc. Natl. Acad. Sci. USA **99:**5110–5114.
46. **Wade, D., A. Boman, B. Wahlin, C. M. Drain, D. Andreu, H. G. Boman, and R. B. Merrifield.** 1990. All-D amino acid-containing channel-forming antibiotic peptides. Proc. Natl. Acad. Sci. USA **87:**4761–4765.
47. **Wiegand, H., B. Wirz, A. Schweitzer, G. Gross, M. I. Perez, H. Andres, T. Kimmerlin, M. Rueping, and D. Seebach.** 2004. Pharmacokinetic investigation of a ^{14}C-labelled beta 3/alpha tetrapeptide in rats. Chem. Biodivers. **1:**1812–1828.
48. **Xiong, Y. Q., M. R. Yeaman, and A. S. Bayer.** 1999. In vitro antibacterial activities of platelet microbicidal protein and neutrophil defensin against *Staphylococcus aureus* are influenced by antibiotics differing in mechanism of action. Antimicrob. Agents Chemother. **43:**1111–1117.
49. **Yang, D., Z. H. Liu, P. Tewary, Q. Chen, G. de la Rosa, and J. J. Oppenheim.** 2007. Defensin participation in innate and adaptive immunity. Curr. Pharm. Des. **13:**3131–3139.
50. **Yaron, S., T. Rydlo, D. Shachar, and A. Mor.** 2003. Activity of dermaseptin K_4-S4 against foodborne pathogens. Peptides **24:**1815–1821.
51. **Zasloff, M.** 2002. Antimicrobial peptides of multicellular organisms. Nature **415:**389–395.